**Steel and Composite Structures**, *Vol. 29, No. 6 (2018) 689-701*
DOI: https://doi.org/10.12989/scs.2018.29.6.689


# Behavior of steel-concrete jacketed corrosion-damaged RC columns subjected to eccentric load

Jiyue Hu [a], Hongjun Liang [b] and Yiyan Lu [*]

*School of Civil Engineering, Wuhan University, Wuhan 430072, China*

(*Received December 3, 2017, Revised October 30, 2018, Accepted December 18, 2018*)

**Abstract.** Corrosion of steel reinforcement is a principal cause of deterioration of RC columns. Making these corrosion-damaged columns conform to new safety regulations and functions is a tremendous technological challenge. This study presented an experimental investigation on steel-concrete jacketed corrosion-damaged RC columns. The influences of steel jacket thickness and concrete strength on the enhancement performance of the strengthened specimens were investigated. The results showed that the use of steel-concrete jacketing is efficient since the stub strengthened columns behaved in a more ductile manner. Moreover, the ultimate strength of the corrosion-damaged RC columns is increased by an average of 5.3 times, and the ductility is also significantly improved by the strengthening method. The bearing capacity of the strengthening columns increases with the steel tube thickness increasing, and the strengthening concrete strength has a positive impact on both bearing capacity, whereas a negative influence on the ductility. Subsequently, a numerical model was developed to predict the behavior of the retrofitted columns. The model takes into account corrosion-damage of steel rebar and confining enhancement supplied by the steel tube. Comparative results with the experimental results indicated that the developed numerical model is an effective simulation. Based on extensive verified numerical studies, a design equation was proposed and found to predict well the ultimate eccentric strength of the strengthened columns.

**Keywords:** steel-concrete jacketing; corrosion-damage; retrofit; eccentric compression

## 1. Introduction

Corrosion of steel reinforcement has become a major cause of reducing the service life of many existing reinforced concrete (RC) bridge piers (Maaddawy and Soudki 2003). Due to the corrosion nearly one of every three bridges in the North America is structurally deficient or functionally obsolete (Smith and Virmani 2000). The annual worldwide investment on corrosion related maintenance and repair of RC structures totals $100billion (Li and Melchers 2005). Therefore, determining how to prevent further corrosion and strengthen the corrosion-damaged columns, thereby extending the service life, is a tremendous technological and financial challenge.

Common retrofitting solutions include FRP composite wrapping (Dai *et al*. 2011 and 2015, Liang *et al*. 2018 and 2019, Khan *et al*. 2016), concrete jacketing (Colomb *et al*. 2008), and steel jacketing (Xiao and Wu 2003, Rupp *et al*. 2014). Some composite reinforcement methods, including FRP-steel jacketing (Lu *et al*. 2018), concrete filled FRP-steel jacketing (Zhang *et al*. 2018, Wang *et al*. 2014), and steel-concrete jacketing, have developed rapidly and attracted attentions. Steel-concrete jacketing, as a combined variation of the steel jacketing and concrete jacketing, has jacketing, has been used in this paper to retrofit RC columns. The retrofitting procedure consisted of striping off the protective layer and deteriorated concrete, packing a circular steel tube jacket welded by two pieces of semicircular steel plates and casting repair concrete to make them become an integral. This method can combine the beneficial qualities of steel and concrete materials (Elremaily and Azizinamini 2002). The former possesses the advantages of high tensile strength and ductility while the latter has the advantages of high compressive strength and stiffness (Gao *et al*. 2017). Meanwhile, the strength, stiffness and the deformation capacity of the damaged columns can be enhanced due to the effective confinement given by the exterior steel tube. Moreover, the presence of concrete infill prevents the steel tube from local buckling. Therefore, this retrofitting method is recognized as being excellent mechanical performance, easy to construct and relatively economical. Chai *et al*. (1991) and Priestley *et al*. (1994a, b) were the first to make an exploratory study of this retrofitting method. However, the diameter of circular RC columns was increased from 610 to 632 mm, with the void filled with grout. As a result, the bearing capacity is mainly borne by the steel jacket and the bearing capacity of the filling material can be neglected. Han *et al*. (2006) and Tao and Han (2007) proposed the method of RC columns strengthened with circular steel-concrete jacket. The diameters of RC columns was increased from 100 to 160 mm. The experimental results indicated that the bearing capacity has been greatly improved by the steel-concrete jacketing and the ductility was also significantly improved.

*Corresponding author, Professor,
E-mail: yylu901@163.com
[a] Ph.D., E-mail: hujiyue123@foxmail.com
[b] Ph.D., E-mail: hongjunliang8@163.com


http://www.techno-press.org/?journal=scs&subpage=6 ISSN: 1229-9367 (Print), 1598-6233 (Online)

Sezen and Miller (2011) conducted comparison tests on circular concrete-steel jacket, concrete jacket and FRP jacket retrofitted RC columns. The test results show that the steel-concrete jacket strengthening is more effective than the concrete jacket and the FRP jacket strengthening to improve the specimen stiffness, member strength and ductility because of the sufficient confinement. Lu *et al*. (2015a, b) carried out an experimental investigation to compare the capacity of RC columns strengthened with circular steel-concrete jacket and square steel-concrete jacket. The results indicated the circular steel-concrete jacket could provide more effective confinement than the square jacket, while the square jacket possessed more convenient construction and simpler joint connection. The diameters or widths were increased from 150 to 220 mm for both square and circular RC columns. He *et al*. (2016, 2017 and 2018) performed experimental and numerical studies on the behavior of circular steel-jacket retrofitted RC columns with preload effects and the results illustrated that by using the steel-jacket retrofitting approach with recycled aggregate concrete, the initial stiffness, ultimate strength, deformation ductility and energy dissipation ability of the columns are improved significantly. Moreover, the effects of preload levels on the axial compressive strength of the retrofitted column can be negligible while the eccentric compressive strength increases with the preloads increasing. Successful application of the steel tube and sandwiched concrete jacketing technique has been reported in the strengthening of deficient CFST columns of a blast furnace (Zhong 2003) and fire-damaged CFST columns of a glass furnace (Lin *et al*. 1997) in China.

However, few experimental investigations were performed on steel-concrete jacketed corrosion-damaged RC columns. Possible reason is that the exposed steel jacket is considered to be susceptible to corrosion. With the rapid development of the technology of steel jacket corrosion resisting, such as many effective inhibitors (Yadav *et al*. 2015, and Bentiss *et al*. 2011), steel jacket can resist corrosion ten years or more time in the marine environment. It is becoming possible that using steel-concrete jacketing to upgrade corroded RC columns. Therefore, this paper would perform an experimental and a numerical investigation on the behavior of steel-concrete jacketed corrosion-damaged RC columns under eccentric load. In the experimental investigation, twenty-one circular RC columns would be corroded through an external current technique within a reasonable time, strengthened with steel-concrete jacket, and tested to failure under eccentric load. The degradation of RC columns due to steel corrosion and the enhancement due to strengthening would be investigated. Failure modes, ultimate strengths, flexural rigidity and ductility of the strengthened columns will be described and analyzed. In the numerical investigation, the complete load–deflection response and the ultimate strengths of the strengthened columns under eccentric loads will be predicted and then compared with the experimental results. Finally, based on massive verified numerical results, a design equation would be developed to calculate the ultimate eccentric strength of the strengthened columns which can help engineers to design for strengthening.

## 2. Experimental program

### *2.1 Test specimens*

Twenty-one circular RC columns were fabricated and test. The RC columns have a clear length ($L$) of 657 m with a cross-section of 150 mm diameter ($D$) as shown in Fig. 1. The columns were reinforced with six 12 mm diameter longitudinal bars and transversely reinforced with 6 mm diameter hoops, spaced at 150 mm. The average yield strength ($f_y$) of the steel, the tensile strength ($f_u$) and elongation rate obtained from tensile tests are listed in Table 1. As model columns simulating deficient columns, the RC columns were poured with normal vibrated concrete (NVC) whose design strength was low to 30 MPa. The mix proportions and average compressive strength of concrete cube after 28 days curing are listed in Table 2.

### *2.2 Accelerated steel corrosion tests*

An external current was utilized to induce corrosion in test specimens within a reasonable time as shown in Fig. 2. The specimens were placed in a water tank containing 5% salt solution. The longitudinal bars were used as the anode. Several stainless iron plates immersed in the bank were used as cathode, through which a constant current of 1.0 mA/cm$^2$ was applied. The predetermined nominal corrosion level was controlled by the volume of integrated electric current and estimated by Faraday's law as follows

$$t = \frac{2F\eta m}{MI} \tag{1}$$

where $t$ = time (second), F = Faraday's constant (96485 amperes/seconds), $\eta$ = nominal corrosion level (%), $m$ = mass of non-corroded steel bars (g), $M$ = atomic weight of metal (56g for Fe), $I$ = current (amperes).

Based on the previous research (Fang and Lundgren 2004 and 2006a, Fang *et al*. 2006b, Lu *et al*. 2018, and Li *et al*. 2018), nominal corrosion degree ($\eta$) of the corrosion-damaged was set from 0 to 25%. When reaching the destined corrosion ratio, the specimens would be taken from the tank. The draws of the cleaned RC columns surface and the corrosion cracks on the surface were shown in Fig.3. In the figure, only a little mixture of relatively red-black corrosion products and no apparent cracks were found on the surface of the RC specimen with 3% nominal corrosion level. When the nominal corrosion level was beyond 6%, a lot of red–black corrosion products and visible corrosion cracks could be observed in test specimens. It was also seen that the corrosion products concentrated on or close to the main corrosion cracks. The main crack which exhibited parallel to the steel reinforcing bars developed wider and longer with the electrifying time increases. The main crack width was measured by a microscope that provides a resolution of ±0.01 mm. The maximum corrosion crack width of the RC specimen with 6%, 10%, 15% and 20% nominal corrosion level were 0.41 mm,1.25 mm, 2.60 mm and 3.13 mm, respectively. The maximum crack width of the RC specimen with 25% is beyond 4 mm which cannot be measured. Meanwhile, flaking of massive concrete was observed in the end of the RC specimen with 25% corrosion level. The corrosion crack length of the 6% corrosion specimen took up about 2/3 length of the entire column. However, the crack would occupy the entire column when the corrosion was beyond 10%. These phenomena implied that the cover concrete of the RC columns was seriously damaged due to serious rust stains.

### 2.3 Strengthening procedure

The strengthening procedure consisted of striping off the protective layer and deteriorated concrete, packing a circular steel tube jacket welded by two pieces of semi-circular steel plates and casting repair concrete to make them become an integral. In practical engineering, there is a necessary process that some effective inhibitors or anticorrosive paint will be smeared on the outside surface of


(a) RC


(b) SRC

Fig. 1 Configuration of RC specimens and strengthened specimens

Table 1 Material properties of steel material

| Steel | d1 or t (mm) | fy (MPa) | fu (MPa) | Elongation rate (%) |
|---|---|---|---|---|
| Hoop Rebar | 6.0 | 310 | 356 | 25.0 |
| Longitudinal Rebar | 12.0 | 458 | 615 | 21.9 |
| t2 Steel tube | 2.10 | 394 | 538 | 25.4 |
| t3 Steel tube | 2.80 | 355 | 482 | 27.6 |
| t4 Steel tube | 3.80 | 342 | 475 | 22.0 |

* Note: $d_1$ is diameter of the rebar. $t$ is actual wall thickness of the steel tubes

Table 2 Mix proportions and average compressive strength of concrete

| Concrete | Mix proportions (kg·m$^{-3}$) | | | | | | | Compressive strength $f_{cu}$ (MPa) | Slump flow (mm) |
|---|---|---|---|---|---|---|---|---|---|
| | Water | 42.5R cement | River Sand | Coarse aggregate | Expansive agent | Water reducer | Fly ash | | |
| C25 NVC | 218.8 | 336.7 | 733.9 | 1198.5 | - | - | - | 31.52 | - |
| C30 SCC | 184.7 | 348.6 | 923.7 | 833.1 | 4.4 | 0.6 | 149.9 | 36.63 | 665 |
| C40 SCC | 178.5 | 396.6 | 813.0 | 868.5 | 5.0 | 0.9 | 170.5 | 44.87 | 658 |
| C50 SCC | 150.1 | 428.7 | 797.4 | 857.5 | 5.4 | 1.6 | 184.4 | 54.69 | 700 |

steel tube to prevent corrosion. However, the process was omitted in experiment since it does not affect the short-term mechanical properties of the strengthened columns. The diameter of the strengthened specimens is 219 mm as shown in Fig. 1. The gap between the corrosion-damaged RC columns and the steel tube jacket was as low as 35 mm so that the steel tube cannot be filled uniformly with NVC concrete. Therefore, the self-compacting concrete (SCC) was used which allows pouring concrete without vibration even in the presence of a highly dense reinforcement or novel form of construction (Han and Yao 2004, Holschemacher 2004). The mix proportions of the SCC determined by trial mixtures are given in Table 2 where the slump flow and the average compressive strength of the SCC are also listed. The actual steel tube thickness, the average yield strength ($f_y$), the tensile strength ($f_u$) and elongation rate of the steel tubes obtained from tensile tests are shown in Table 1.

In summary, main parameters for the tests are set as follows: (1) nominal corrosion degree ($\eta$) which changes from 0 to 25%; (2) nominal steel tubes thickness ($t$) which varies from 2 mm to 4 mm; (3) designed strength grade of strengthening concrete (C) which includes C30, C40 and C50; (4) initial eccentricity ($e_0$) which changes from 15 to 45 mm. All the specimens with varied parameters were divided in two groups including 8 corrosion-damaged RC columns without any strengthening (W group) and 13 steel-concrete retrofitted corrosion-damaged RC columns (S group) as listed in Table 3. The nomenclature of the specimens in this test is: Xt-C-$\eta$-$e_0$ (i.e., S3-C40-15%-e30), where $X$ stands for strengthening method, "$t$" is the nominal wall thickness of steel tube in mm, "$C$" is the designed

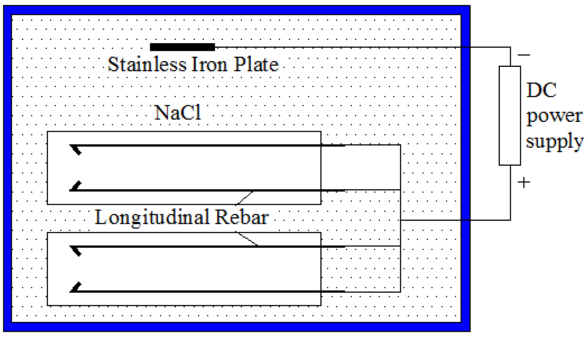


(a) Schematic drawing

(b) Photograph

Fig. 2 Vertical view of accelerated corrosion device


(a) General crack situation

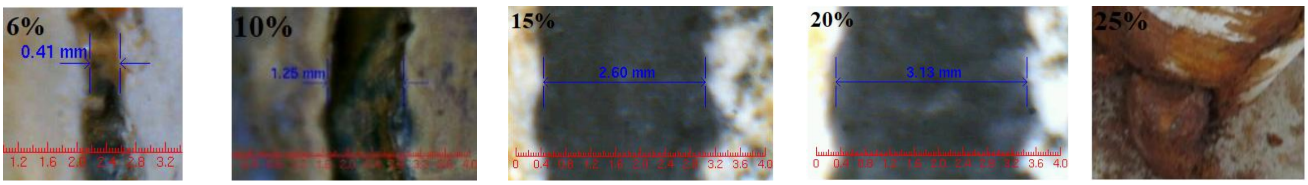


(b) Maximum crack width

Fig. 3 The corrosion cracks of RC specimens with different nominal corrosion level

Table 3 Geometrical and material parameters for all test specimens

| Specimen | $D \times t \times L$(mm) | $\eta_1$ | $N_e$ (kN) | $N_f$ (kN) | $N_f/N_e$ | $N_p$ (kN) | $N_p/N_e$ |
|---|---|---|---|---|---|---|---|
| W-C25-0%-e0 | 150×0×657 | 0% | 854 | - | - | - | - |
| W-C25-0%-e30 | 150×0×657 | 0% | 382 | -- | - | - | - |
| W-C25-3%-e30 | 150×0×657 | 3.81% | 358 | - | - | - | - |
| W-C25-6%-e30 | 150×0×657 | 5.49% | 312 | - | - | - | - |
| W-C25-10%-e30 | 150×0×657 | 8.04% | 238 | - | - | - | - |
| W-C25-15%-e30 | 150×0×657 | 12.69% | 232 | - | - | - | - |
| W-C25-20%-e30 | 150×0×657 | 15.19% | 206 | - | - | - | - |
| W-C25-25%-e30 | 150×0×657 | 20.60% | 0 | - | - | - | - |
| S3-C40-0%-e30 | 219×2.80×657 | 0% | 1610 | 1552 | 0.964 | 1478 | 0.918 |
| S3-C40-6%-e30 | 219×2.80×657 | 5.49% | 1542 | 1478 | 0.958 | 1447 | 0.938 |
| S3-C40-10%-e30 | 219×2.80×657 | 8.04% | 1492 | 1443 | 0.967 | 1431 | 0.959 |
| S3-C40-15%-e30 | 219×2.80×657 | 12.69% | 1418 | 1380 | 0.973 | 1401 | 0.988 |
| S3-C40-20%-e30 | 219×2.80×657 | 15.19% | 1312 | 1346 | 1.026 | 1383 | 1.054 |
| S3-C40-25%-e30 | 219×2.80×657 | 20.60% | 1272 | 1274 | 1.002 | 1341 | 1.054 |
| S2-C40-10%-e30 | 219×2.10×657 | 8.04% | 1394 | 1341 | 0.962 | 1383 | 0.992 |
| S4-C40-10%-e30 | 219×3.80×657 | 8.04% | 1670 | 1616 | 0.968 | 1580 | 0.946 |
| S3-C30-10%-e30 | 219×2.80×657 | 8.04% | 1402 | 1361 | 0.971 | 1340 | 0.956 |
| S3-C50-10%-e30 | 219×2.80×657 | 8.04% | 1612 | 1541 | 0.956 | 1581 | 0.981 |
| S3-C40-10%-e0 | 219×2.80×657 | 8.04% | 2146 | - | - | 2087 | 0.973 |
| S3-C40-10%-e15 | 219×2.80×657 | 8.04% | 1718 | 1676 | 0.976 | 1698 | 0.988 |
| S3-C40-10%-e45 | 219×2.80×657 | 8.04% | 1298 | 1234 | 0.951 | 1237 | 0.953 |

*Note: $\eta_1$ = actual average corrosion degree; $N_e$ = experimental ultimate strength; $N_f$ = ultimate strength predicted by fiber element model; $N_p$ = ultimate strength calculated by design formula

strength grade of strengthening concrete in MPa, "$\eta$" is the nominal corrosion degree of steel rebar, and "$e_0$" means the initial eccentricity.

### *2.4 Eccentric loading tests*

All the tests were performed on a 5000 kN capacity universal testing machine. Fig. 4 gave the schematic view of the setup and instrument layout. In the test, the eccentric load was applied through a triangular hinge to simulate a desired pinned support, which allows the specimen to rotate but restrains its translation at the same time. A male plate was placed at the center of the specimens. Another female plate was positioned on the male plate according to the required eccentricity. The load was applied in an increment of 50 kN before peak load. Each load interval was maintained for 2~3 min. The load was applied slowly and continually near and after the peak load, until final failure occurred to investigate the post-peak behavior of the specimens. A force transducer was placed to accurately measure the applied axial load in real-time below the specimens. Two linear variable displacement transducers (LVDTs) were placed to measure the axial shortening on two sides of the specimens. Three LVDTs were used to symmetrically measure the lateral deformation of the column at the mid-height (0.5 L) and quarter-heights (0.25 L, 0.75 L). Eight electrical strain gauges were glued to measure the axial and transverse strains of four locations 0°,90°, 180°, and 270° on the external surface of the circular steel tubes at mid-height. A computerized data-acquisition system was used to collect the experimental data.

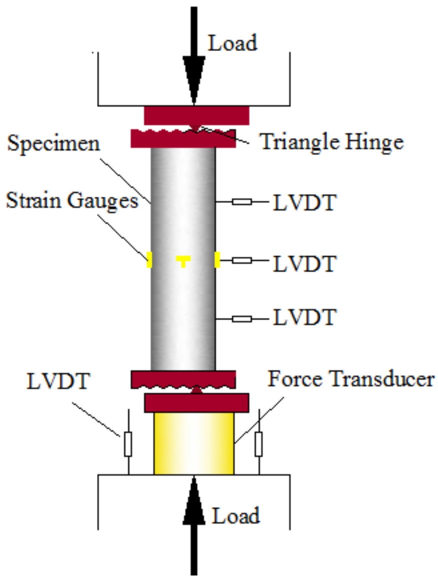


Fig. 4 Test setup and instrumentation

## 3. Results and discussion

### 3.1 Failure modes

Before the loading, two 100 mm wide and 500 mm long CFRP strips were wrapped at the top and bottom of all RC columns without any strengthening (WRC columns) to prevent premature end failure as shown in Fig. 5. The typical failure mode of the WRC columns was the material failure. The first phenomenon was observed as longitudinal cracking of the cover concrete when the applied load increased up to 60%~70% of the ultimate load. And then, the cover concrete was spalling and flaking due to the development of cracks in the concrete surrounding the longitudinal reinforcements. After the ultimate load, the applied load decreases rapidly. When the test was terminated, the lateral deformation and axial shortening can be clearly observed. The computer data showed that the maximum axial shortening and lateral deflection of the WRC columns were 0.82 mm and 1.09 mm, respectively.

For the steel-concrete retrofitted corrosion-damaged RC columns (SRC columns), the stub strengthened columns behaved in a relatively ductile manner. The typical failure mode was the outward local buckling in the compression

W-C25-0%-e30 W-C25-3%-e30 W-C25-6%-e30 W-C25-10%-e30 W-C25-15%-e30 W-C25-20%-e30

S3-C40-0%-e30 S3-C30-10%-e30 S3-C40-10%-e45 S3-C40-15%-e30 S3-C40-10%-e15 S4-C40-10%-e30

Fig. 5 Typical failure modes of specimens

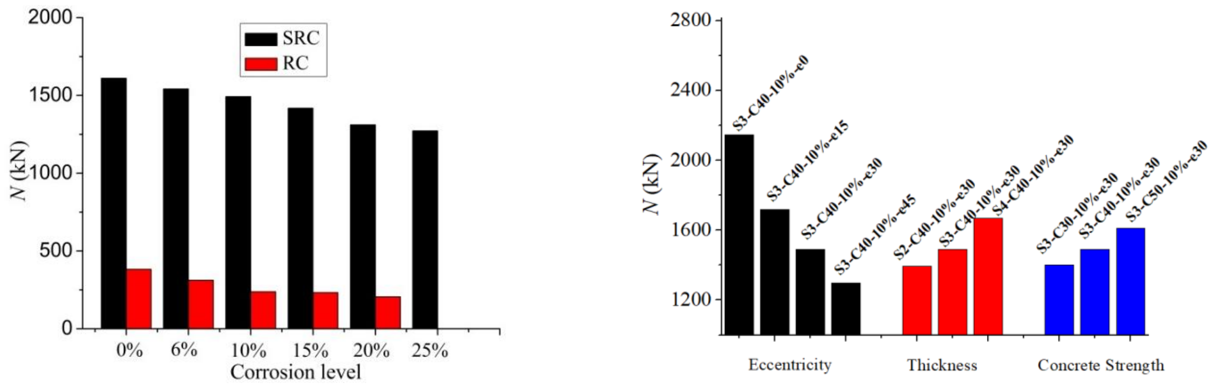


(a) RC and SRC with different corrosion level (b) SRC with different geomietic parameters

Fig. 6 Ultimate strengths of all the specimens

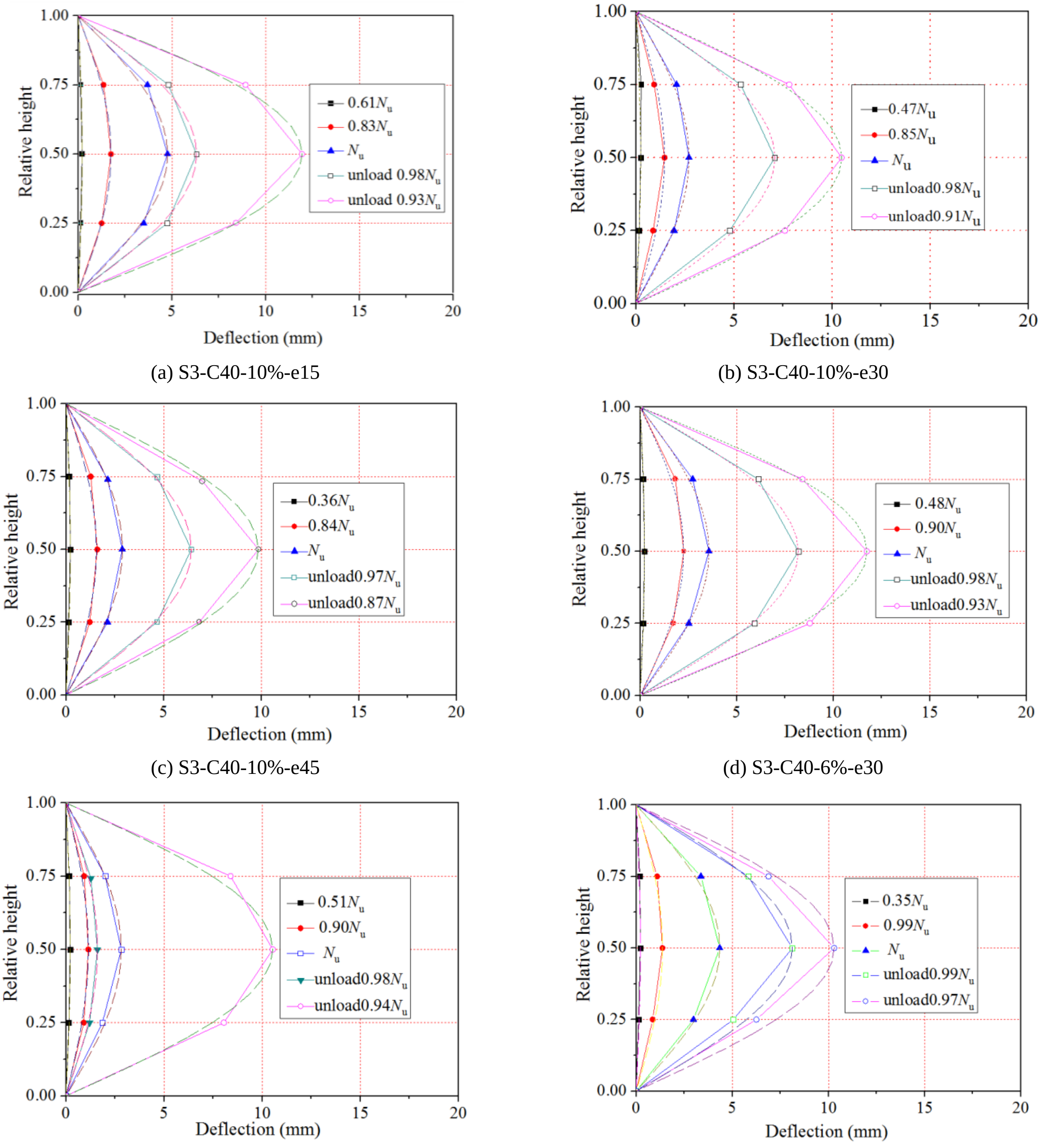


(a) S3-C40-10%-e15 (b) S3-C40-10%-e30

(c) S3-C40-10%-e45 (d) S3-C40-6%-e30

(e) S3-C40-15%-e30 (f) S3-C40-20%-e30

Fig. 7 Lateral deformation along typical specimens' height

part due to extrusion of the filled concrete. The local buckling was firstly observed about 70%~80% of the maximum load and became more serious as the load was increased. After the ultimate load, the applied load was stabilized at a certain loading level while the deformation was still aggravating. When the test was terminated, two visible bulges were observed near the quarter heights of the specimens. The bulges were at the lower and the upper compression part of the steel tube. After the steel pipe was broken, it was found that part of the concrete at this location was crushed. Meanwhile, the specimens showed an overall serious bending deformation. The computer data showed that the maximum axial shortening was 3.42 mm and the maximum lateral deflection of the SRC column was apparent up to even beyond 22.66 mm which revealed that steel-concrete jacketing could increase the deformation capacity of the RC columns.

### *3.2 Ultimate strengths*

Fig. 6 compared the ultimate strengths of specimens to investigate the degradation of corrosion-damaged RC columns and enhancement of strengthened columns. The results reveal that: (1) the structural strengths of the RC columns have been seriously weakened due to corrosion. The ultimate strengths of W-C25-3%-e30, W-C25-6%-e30, W-C25-10%-e30, W-C25-15%-e30 and W- C25-20%-e30 were 6.28%, 18.32%, 37.70%, 39.27% and 46.07% respectively less than that of W-C25-0%-e30. For more severe corroded specimen (W-C25-25%-e30), it was considered be no bearing capacity due to flaking of the massive concrete cover. (2) steel-concrete jacketing could increase the bearing capacity of the corrosion-damaged RC columns significantly. The mean strength of the strengthened columns was 5.3 times of the damaged RC columns. (3) The wall thickness of steel tubes has an extremely positive effect on the ultimate strength of strengthened columns. The ultimate strengths of S4-C40-10%-e30 and S3-C40-10%-e30 were 7.03% and 19.80% respectively more than that of S2-C40-10%-e30. (4) The ultimate strength increases slightly with increases in the concrete compressive strengths. The ultimate strengths of S3-C50-10%-e30 and S3-C40-10%-e30 are 6.42% and 14.98% respectively more than that of S3-C30-10%-e30. (5) The initial eccentricity has a remarkably detrimental effect on the ultimate strength of strengthened columns. The ultimate strengths of S3-C40-10%-e45, S3-C40-10%-e30 and S3-C40-10%-e15 were 39.52%, 30.48% and 19.94% less than that of S3-C40-10%-e0, respectively. In conclusion, the structural strengths of the RC columns were seriously degraded due to corrosion and enhanced by steel-concrete jacketing.

### *3.3 Load-lateral deflection*

Fig. 7 presented the typical curves of the applied load ($N$) versus lateral deflection ($f$) relationships along the strengthened specimens' height. The visible lateral deflection was firstly measured on S3-C40-10%-e45 when the applied load was up to approximately 28% of the ultimate load for the SRC columns. The visible deflection of others specimens which have the smaller initial eccentricity are observed about 40%-50% of the ultimate load. Beyond this load level, the deflection increased more rapidly as the load increases. This is because the lateral deflection would generate a secondary moment ($M = Nf$) which could magnify the lateral deflection. Moreover, the graphs showed that the deflection at the mid-height ($f_{\mathrm{m}}$) is greater than those at the two quarter-heights. The deflected shape ($f$) of the compressed column showed good agreement with the assumed half-sine curve at every load level. Therefore, the deflected shape can be expressed by the following equation

$$f = f_m \sin\left(\frac{\pi z}{L}\right) \tag{2}$$

### *3.4 Load-deflection at mid-height*

The above analysis indicated that the mid-height section is the most critical section because it bears the largest moment. Therefore, the applied loads ($N$) versus deflection curves at mid-height ($f_{\mathrm{m}}$) of the specimens are studied as shown in Fig. 8. Fig. 8(a) presented the $N$-$f_{\mathrm{m}}$ curves of the W group and S group specimens with different corrosion degrees ($\eta$), in which the curves with adjacent $\eta$ are placed on both sides of the vertical axis to distinguish them more clearly. In the initial stage of loading, all the specimens were in the elastic stage, and the $N$-$f$ curves were close to linearity. However, it was apparent that the $N$-$f$ curves of S group specimens exhibit greater slope and longer linear stage. Moreover, loads of S group specimens could keep constant at a certain loading level after ultimate load. These indicated that the strengthened columns behave a greater flexural rigidity and are more ductile than the corrosion-damaged RC columns. Meanwhile, it is found that there is no obvious difference in the slope of elastic stage between the strengthened columns with different corrosion degrees. It implied that the corrosion degree has no significant influence on the flexural rigidity. Fig. 8(b) showed the $N$-$f_{\mathrm{m}}$ curves of the strengthened specimens with different initial eccentricity ($e_0$). The load eccentricity demonstrated an adverse influence on the strength of the specimens while it had no significant influence on the ductility. Figs. 8(c) and (d) compared the $N$-$f_{\mathrm{m}}$ curves of the strengthened specimens with different nominal wall thicknesses of steel tubes and compressive strengths of strengthening concrete. It can be found from the comparison between the specimens, such as specimens with 4 mm and 2 mm thickness steel tubes, that the applied load decreased more slowly as the wall thickness increases after the failure load. Furthermore, it has also been noted in Fig. 8(d) that the load of the specimens with lower concrete strength could keep constant at a higher loading level after the failure load. It can be concluded that a strengthened column with a thinner wall of the steel tubes and a higher strength concrete has a poorer ductility. These are the reasons that many design codes, such as the Euro code4, restrict the maximum of $D$/t and limit the use of high strength concrete to guarantee an excellent ductile behavior.

## 4. Numerical analysis

### *4.1 Fiber element discretization*

The fiber element method is a simple and yet efficient numerical technique for predicting the ultimate strengths of composite columns (Liang 2011 and Liu 2006). In the analysis, the concrete and the steel need to be discretized into a number of fibers as depicted in Fig. 9. In this study, the number of the element was set as 10000 (= 200×50) considering reasonable accuracy and calculation speed.

### *4.2 Strain of element*

It is assumed that there is no slippage between the strengthened section and the RC column so that the cross section remained plane, and the steel tube and the concrete deformed compatibly when the column deflects, resulting in a linear strain distribution. Therefore, the strain for the centroidal area of the element $i$ was calculated as

$$\varepsilon_i = \varepsilon_0 + \Phi y_i \tag{3}$$

where $\varepsilon_0$ is the strain at the centroid axis of the cross section, $y_{\mathrm{i}}$ is the coordinate of the fiber element, and $\Phi$ is

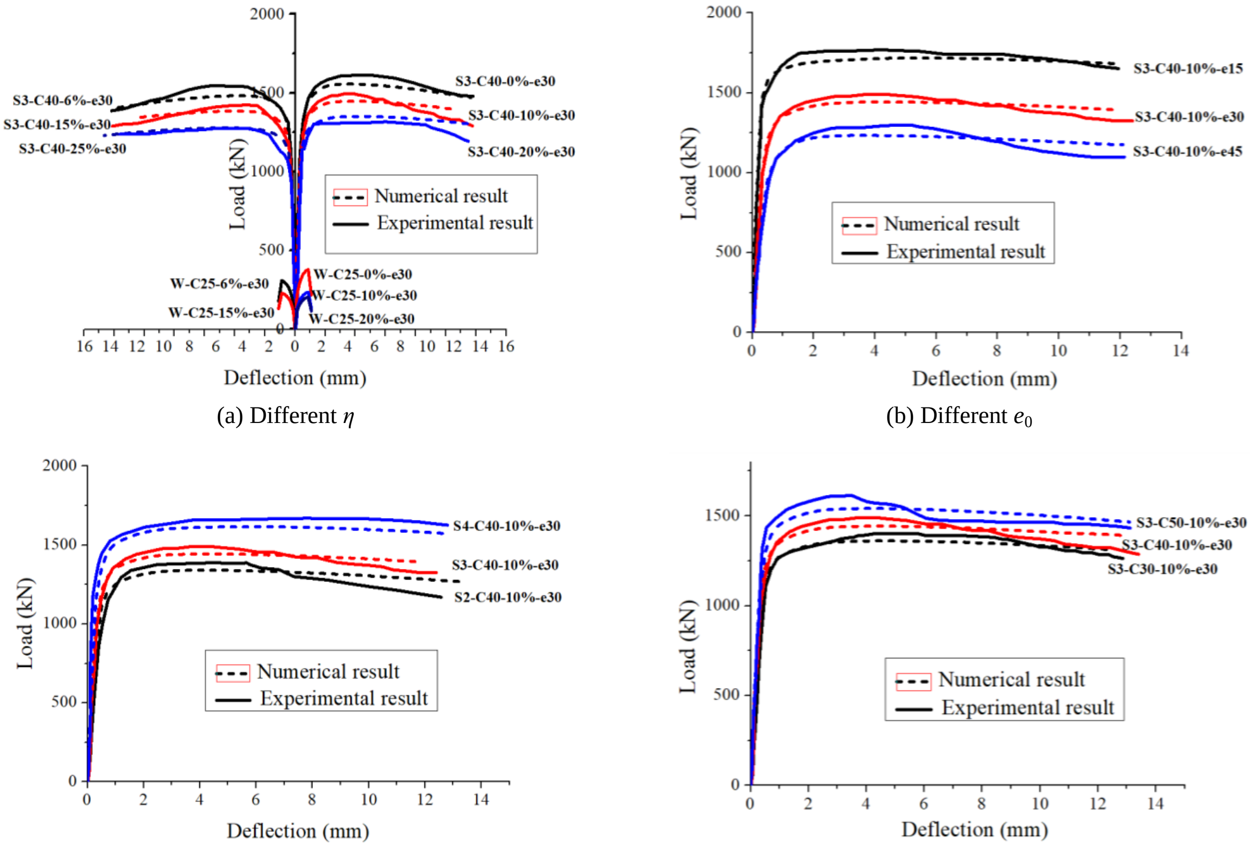


(a) Different $\eta$ (b) Different $e_0$

(c) Different $t$ (d) Different $C$

Fig. 8 Load-deflection curves of specimens with different parameters

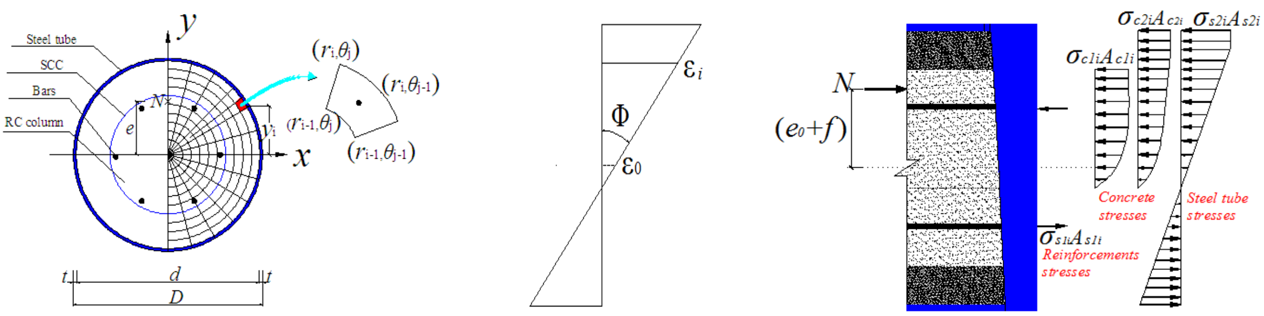


(a) Section discretization (b) Strain distribution (c) Stress distribution

Fig. 9 Strain and stress distribution

the curvature of the column. The $\Phi$ at the mid-height of the columns can be obtained from Eq. (4) as

$$\Phi = \frac{\partial^2 f}{\partial z^2}\bigg|_{z=\frac{L}{2}} = (\frac{\pi}{L})^2 f_m \sin(\frac{\pi z}{L})\bigg|_{z=\frac{L}{2}} = (\frac{\pi}{L})^2 f_m \qquad (4)$$

### 4.3 Stress of element

In order to obtain the stress of all the elements, the stress–strain relation of the steel and the concrete need to be determined. In this study, the stress-strain relationship described in Qiao *et al*. (2015) was used, which considers the hardening stage of steel given as

$$\sigma = \begin{cases} E_s \varepsilon & (\varepsilon < \varepsilon_y) \\ f_y & (\varepsilon_y \le \varepsilon < \varepsilon_{sh}) \\ f_y + (1 - e^{(\varepsilon_{sh}-\varepsilon)/w})(1.01 f_u - f_y) & (\varepsilon_{sh} < \varepsilon) \end{cases} \qquad (5)$$

$$w = 0.032(400 / f_y)^{1/3} \qquad (6)$$

in which $f_y$, $E_s$, $\varepsilon_y$ and $\varepsilon_{sh}$ are the yield stress, the Young's modulus, the yield strain and strain until hardening stage of steel, respectively. As can be seen in the Fig. 10, the proposed rebar material model and experimental results are similar.

Many studies have demonstrated that corrosion might decrease yield and ultimate tensile strengths of steel rebar while slightly reduce elastic modulus (Qiao *et al*. 2015, Lee and Cho 2009, Cairns *et al*. 2005, Almusallam 2001, and Zhang *et al*. 2012). An empirical correlation with actual corrosion degree $\eta_1$ (%) has been proposed in the literature to estimate the residual tensile capacity

$$\begin{cases} f_y = (1.0 - \alpha_y \cdot \eta_1) f_{y0} \\ f_u = (1.0 - \alpha_u \cdot \eta_1) f_{u0} \end{cases} \tag{7}$$

$$\eta_1 = \frac{\sum (m_{0i} - m_{ci})}{\sum m_{0i}} \tag{8}$$

in which values of coefficient $\alpha_y$ = 0.012~0.017 and $\alpha_u$ = 0.011~0.018, $\eta_1$ is the actual corrosion degree and listed in Table. 3, $m_{0i}$ is the mass of non-corroded rebar *i*, $m_{ci}$ is the mass of cleaned corroded rebar *i*.

In order to determine the accurate stress-strain relationship of the corroded rebar, the rebar extracted from the corrosion-damaged RC column, were subjected to tensile tests. The tensile results, in terms of nominal stress and strain, were reported in Fig. 10. By comparing the calculated results, it is found that the most consistent calculation results with experimental results will be achieved when $\alpha_y$ = 0.012 and $\alpha_u$ = 0.011. Moreover, a special phenomenon was observed that the yielding plateau was constantly shorter as $\eta$ increases, and even completely disappeared when the corrosion degree was beyond 15%. The similar phenomenon was also observed by Qiao *et al*. (2015) and Zhang *et al*. (2012). However, no formula was proposed to calculate the $\varepsilon_{sh}$ of corroded rebar. In this study, $\varepsilon_{sh}$ was assumed to be linear decrease with the increase of corrosion degree and expresses as

$$\varepsilon_{sh} = \begin{cases} \frac{f_y}{E_s} + (\varepsilon_{sh0} - \frac{f_{y0}}{E_{s0}})(1 - \frac{\eta}{15}) & (\eta \le 15) \\ 0 & (\eta > 15) \end{cases} \tag{9}$$

in which $f_{y0}$, $E_{s0}$ and $\varepsilon_{sh0}$ are the yield stress, the Young's modulus and strain before hardening stage of non-corroded rebar, respectively. The revised rebar material model was compared with the experimental results as shown in the Fig. 10. The predictions agree well with the test results.

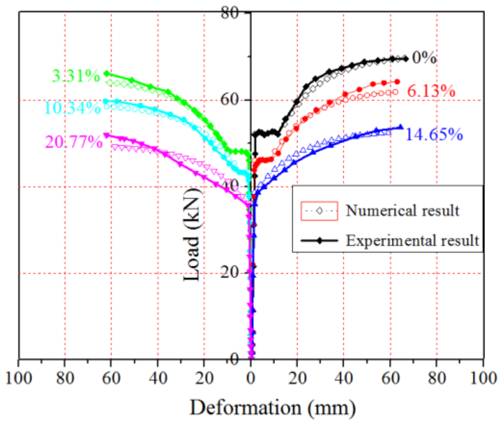

Fig. 10 Stress-strain relation of the steel rebar with different corrosion level

As previously described, the cover concrete of corroded RC columns will be damaged due to the cracks once the nominal corrosion level was beyond a limit value. The damaged concrete of RC columns would gradually withdraw from work and cannot continue to bear load with the cracks widen. However, after strengthened by steel-concrete jacketing, the damaged concrete will be confined by the steel tube. The confinement subjected the damaged concrete to tri-axial stress, thereby recovering its strength and making it return to work (He *et al*. 2017 and 2018). The tri-axial stress-strain relationship for the confined concrete was reported in Han *et al*. (2007)

$$y = \begin{cases} 2x - x^2 & (x \le 1) \\ \frac{x}{\beta \cdot (x-1)^2 + x} & (x > 1) \end{cases} \tag{10}$$

where : $x = \varepsilon/\varepsilon_0$, $y = \sigma/\sigma_0$, $\sigma_0 = f_c'$, $\varepsilon_0 = \varepsilon_c + 800\xi^{0.2}$, $\varepsilon_c = 1300 + 12.5 f_c'$, $\xi = A_{s2} f_{y2}/(A_{c1} f_{ck1} + A_{c2} f_{ck2})$, $\beta = (2.36 \times 10^{-5})^{[0.25+(\xi-0.5)^{\wedge}7]} \times (f_c')^{0.5} \times 0.5$, $A_{s2}$, $f_{y2}$ are the cross-sectional area and the yield stress of the steel tube, $A_{c1}$ and $A_{c2}$ are the cross-sectional areas of the RC column and strengthening concrete, $f_{ck1}$ and $f_{ck2}$ are the nominal strengths of RC column concrete and strengthening concrete. In the analysis, the tensile strength of concrete is negligible. The typical $\sigma$-$\varepsilon$ curve for the confined concrete was drawn in Fig. 11. It is found that the $\sigma$-$\varepsilon$ curve has a descent stage after the strain exceeds $\varepsilon_0$ when $\xi < \xi_0$, whereas the stress keeps constant at a certain level when the confinement factor is large enough.

The effects of concrete deterioration could be taken into account by following formula (Biondini and Vergani 2012)

$$f_c' = [1 - \eta_c(\eta_1)] f_{c0}' \tag{11}$$

in which $f_{c0}'$ is the strength of undamaged concrete. $\eta_c(\eta_1)$ is strength damage function which provides a measure of concrete damage in the range [0;1]. However, it may be not straightforward to establish a relationship between the damage function $\eta_c(\eta_1)$ and the actual corrosion degree $\eta_1$.

In this study, the authors tried to use the bearing capacity of the test columns ($N_e$) to determine the damage function $\eta_c(\eta_1)$. It was assumed that $N_e$ is proportional to the nominal capacity of the concrete ($N_c$) because the bearing capacity of reinforcements only occupies a small percentage. $N_c$ was divided into two parts: internal and external concrete of the reinforcement cages and expressed by

$$N_c = f_{ci} A_{ci} + f_{ce} A_{ce} = f_{c0} A_{ci} \{1 + \frac{A_{ce}}{A_{ci}} [1 - \eta_c(\eta_1)]\} \tag{12}$$

in which $f_{ci}$ is the strength of the internal concrete. It is slightly affected by steel corrosion and considered to be approximately equal to $f_{co}$. $f_{ce}$ is the strength of the damaged external concrete which is calculated by Eq. (11). $A_{ci}$ and $A_{ce}$ are the cross-sectional areas of the internal and external concrete. Subsequently, the relationship between the damage function $\eta_c(\eta_1)$ and $\eta_1$ could be obtained through regression of test results as shown in Fig. 12.

As for the undamaged original concrete and retrofitted SCC concrete, they will also be constrained by steel tube and in a tri-axial stress state as same as the damaged concrete mentioned above. Therefore, their stress-strain model was also characterized by Eq. (10). However, the peak stress ($\sigma_0$) of these three concretes are different. The $\sigma_0$ of the damaged concrete was calculated by Eq. (11), whereas the $\sigma_0$ of the undamaged original concrete and retrofitted SCC converted by the compressive strength ($f_{cu}$) of the concrete cube in Table 1.

### 4.4 Solution

Under the condition of the known areas and stresses of the steel and concrete elements, the applied load and the bending moment acting on the composite section can be determined as shown in the stress integral Eqs. (13) and (14), respectively

$$N = \sum(\sigma_{c1i}\mathrm{d}A_{c1i} + \sigma_{c2i}\mathrm{d}A_{c2i} + \sigma_{s1i}\mathrm{d}A_{s1i} + \sigma_{s2i}\mathrm{d}A_{s2i}) \quad (13)$$

$$M = \sum(\sigma_{c1i}y_i\mathrm{d}A_{c1i} + \sigma_{c2i}y_i\mathrm{d}A_{c2i} + \sigma_{s1i}y_i\mathrm{d}A_{s1i} + \sigma_{s2i}y_i\mathrm{d}A_{s2i}) \quad (14)$$

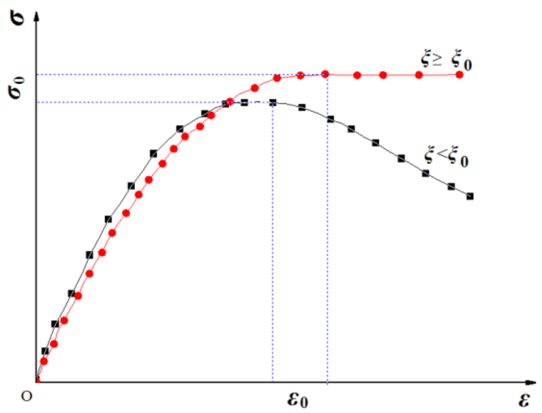


Fig. 11 Stress-strain relation of confined concrete

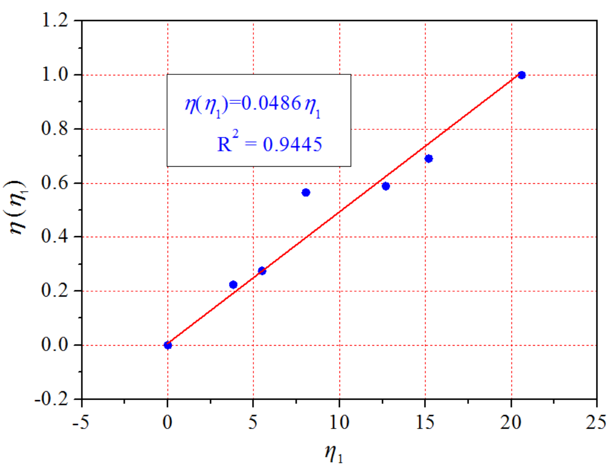


Fig. 12 Regression curve fitting of $\eta c(\eta_1)$

where $\sigma_{c1i}$, $\sigma_{c2i}$, $\sigma_{s1i}$ and $\sigma_{s2i}$ are the longitudinal stresses at the centroid of RC column concrete, strengthening concrete, steel bars and steel tube fiber *i*, respectively. $\mathrm{d}A_{c1i}$, $\mathrm{d}A_{c2i}$, $\mathrm{d}A_{s1i}$ and $\mathrm{d}A_{s2i}$ are the cross-sectional area of RC column concrete, strengthening concrete, steel bars and steel tube fiber *i*.

The equilibrium is maintained at the mid-height of the compressed column and expressed by

$$M = N(e_0 + f_m) \quad (15)$$

In Eqs. (13)-(15), $\varepsilon_0$, $M$, $N$, $e_0$, $f_m$, are unknown variables to be solved. Thus, $N$-$f_m$ relation for a strengthened column could be obtained when the initial eccentricity $e_0$ is a fixed value. In the aid of computational procedure, the complete load–deflection response and the ultimate strengths of the strengthened columns under eccentric loads would be predicted. The ultimate strengths were listed in Table 3 and the obtained $N$-$f_m$ curves were presented in Fig. 8. It could be observed from Fig. 8 that the numerical model gave a good prediction of the stiffness and conservative prediction of the ultimate strength. Meanwhile, the predicted ultimate strength in Table 3 was averagely 97.3% of the experimental value.

## 5. Simplified design equation

Through the above comparison study between the predicted results and the experimental results, it was found that the fiber element method is suitable for calculating steel-concrete jacketed corrosion-damaged RC columns. Subsequently, the model can be used to carry out numerous parametric calculations, thereby deriving the design formula, which is very useful for engineering design. In our previous study (Lu *et al*. 2015b), the author performed a further derivation and logical induction based on massive numerical calculations to establish a formula for calculating the bearing capacity $N_u$ of steel-concrete jacketed undamaged RC columns under eccentric load, as follows

$$N_u = \begin{cases} \dfrac{1}{1+a/k_1}N_{SC} & (N_u > N_C) \\ k_1 N_{SC} & (N_u \le N_C) \end{cases}$$

$$\begin{cases} a = 0.8 - 0.22\xi^{-0.81} \\ k_1 = \dfrac{2k(1+k-\sqrt{(k^2+2k)})M_{SC}}{N_{sc}e_0} \\ k = \dfrac{e_0\pi^2}{\Phi_0 L^2} \\ M_{SC} = \gamma_m W_{scm} f_{scy} + W_{s1} f_{s1} \\ \gamma_m = 1.34 + 0.48\ln(\xi + 0.1) \\ f_{scy} = (1.18 + 0.85\xi)\cdot f_{ck} \\ \xi = f_{y2}A_{s2} / f_{ck}(A_{c1} + A_{c2}) \\ f_{ck} = (f_{ck1}A_{c1} + f_{ck2}A_{c2})/(A_{c1} + A_{c2}) \\ N_{SC} = f_{scy}\cdot(A_{c1} + A_{c2} + A_{s2}) + f_{y1}A_{s1} \\ N_C = N_{SC}(1-a) \end{cases} \quad (16)$$

where $N_{sc}$ is the bearing capacity of retrofitted columns under axial load, $M_{sc}$ is ultimate bending moment under pure bending, $e_0$ is the initial eccentricity of the applied load, $L$ is the length of the column, $W_{scm}$ and $W_{s1}$ are modulus of bending of circular CFST and steel rebar, respectively, $f_{ck1}$ and $f_{ck2}$ are the characteristic value of compressive strength of RC concrete and strengthening concrete, respectively.

This formula had the potential to be extended for calculating $N_u$ of steel-concrete jacketed corrosion-damaged RC columns under eccentric load due to similar mechanical properties and good applicability of the same fiber element model. In order to consider the influence of steel corrosion, the materials strength in the formula was replaced by the decreased yield strength of corroded steel rebar and the strength of damaged concrete. The ultimate strengths predicted by the modified design formula were listed in Table. 3. It could be seen that the mean of $N_p/N_e$ is 0.977, the coefficient of variation is 0.206, and the maximal error between the calculated ultimate strengths and experimental values is 8%. It suggested that the proposed formula could obtain adequately accurate prediction.

## 6. Conclusions

In the present paper, the degradation of RC columns due to steel corrosion and the enhancement due to steel-concrete jacketing were studied experimentally and numerically. Twenty-one specimens, including eight corrosion-damaged RC columns and thirteen steel-concrete jacketed corrosion-damaged RC columns, were tested to failure under eccentric load. The experimental results demonstrated that this strengthening method is significantly effective in improving mechanical properties since the bearing capacity of the corrosion-damaged RC columns was increased by an average of 5.3 times and the ductility was also significantly enhanced. The enhancement of the strengthening was significantly influenced by the in-filled concrete strength and the steel tube thickness. Subsequently, a fiber element method was used to predict the complete load–deflection response and the ultimate strengths of the strengthened columns under eccentric load, and these calculation results were then compared with the experimental results. Finally, a design formula was proposed for calculating the ultimate strength of the strengthened columns based on massive fiber element models, which takes in account damage of corrosion and enhancement of confinement. Through the comparison with the experimental results, the formula has been found to apply not only to steel-concrete jacketed undamaged RC columns but also to the corrosion-damaged columns.

## Acknowledgments

The tests reported herein were made possible by the financial support from the National Natural Science Foundation of China (Grant no. 51708240 and 51678456).

## References

Almusallam, A.A. (2001), "Effect of degree of corrosion on the propertites of reinforcing steel bars", *Constr. Build. Mater.*, **15**, 361-368.

Bentiss, F., Mernari, B., Traisnel, M., Vezin, H. and Lagrenée, M. (2011), "On the relationship between corrosion inhibiting effect and molecular structure of 2, 5-bis (n-pyridyl)-1, 3, 4-thiadiazole derivatives in acidic media: Ac impedance and DFT studies", *Corros. Sci.*, **53**, 487-495.

Biondini, F. and Vergani, M. (2012), "Damage modeling and nonlinear analysis of concrete bridges under corrosion", In: *Sixth International Conference on Bridge Maintenance, Safety Manag* (*IABMAS 2012*), Stresa, Italy, pp. 8-12.

Cairns, J., Plizzari, G.A., Du, Y.G., Law, D.W. and Franzoni, C. (2005), "Mechanical properties of corrosion-damaged reinforce-ment", *ACI, Struct. J.*, **102**, 256-264.

Chai, Y.H., Priestley, M.N. and Seible, F. (1991), "Seismic retrofit of circular bridge columns for enhanced flexural performance", *ACI Struct. J.*, **88**(5), 572-584.

Colomb, F., Tobbi, H., Ferrier, E. and Hamelin, P. (2008), "Seismic retrofit of reinforced concrete short columns by CFRP materials", *Compos. Struct.*, **82**, 475-487.

Dai, J.G., Bai, Y.L. and Teng, J.G. (2011), "Behavior and modeling of concrete confined with FRP composites of large deformability", *J. Compos. Constr.*, **15**, 963-973.

Dai, J.G., Gao, W.Y. and Teng, J.G. (2015), "Finite Element Modeling of Insulated FRP-Strengthened RC Beams Exposed to Fire", *J. Compos. Constr.*, **19**, 428-432.

Elremaily, A. and Azizinamini, A. (2002), "Behavior and strength of circular concrete-filled tube columns", *J. Constr. Steel Res.*, **58**, 1567-1591.

Fang, C. and Lundgren, K. (2004), "Corrosion influence on bond in reinforced concrete", *Cement Concrete Res.*, **34**(1), 2159-2167.

Fang, C. and Lundgren, K. (2006a), "Effect of corrosion on bond in reinforced concrete under cyclic loading", *Cement Concrete Res.*, **36**(3), 548-555.

Fang, C., Lundgren, K., Plos, M. and Gylltoft, K. (2006b), "Bond behavior of corroded reinforcing steel bars in concrete", *Cement Concrete Res.*, **36**(10), 1931-1938.

Gao, F., Zhu, H.P., Liang, H.J. and Tian, Y. (2017), "Post-fire residual strength of steel tubular T-joint with concrete-filled chord", *J. Constr. Steel Res.*, **139**, 327-338.

Han, L.H. and Yao, G.H. (2004), "Experimental behavior of thin-walled hollow structural steel (HSS) columns filled with self-consolidating concrete (SCC)", *Thin-Wall. Struct.*, **42**, 1357-1377.

Han, L.H., Lin, X.K. and Wang, Y.C. (2006), "Cyclic performance of repaired concrete-filled steel tubular columns after exposure to fire", *Thin-Wall. Struct.*, **44**(10), 1063-1076.

Han, L.H., Yao, G.H. and Tao, Z. (2007), "Performance of concrete-filled thin-walled steel tubes under pure torsion", *Thin-Wall. Struct.*, **45**, 24*36.

He, A., Cai, J. and Chen, Q.J. (2016), "Behaviour of steel-jacket retrofitted RC columns with preload effects", *Thin-Wall. Struct.*, **109**, 25-39.

He, A., Cai, J., Chen, Q.J., Liu, X.P., Xue, H. and Yu, C.J. (2017), "Axial compressive behaviour of steel-jacket retrofitted RC columns with recycled aggregate concrete", *Constr. Build. Mater.*, **141**, 501-516.

He, A., Cai, J., Chen, Q.J., Liu, X.P., Xuang, P.Z. and Tang, X.L. (2018), "Seismic behaviour of steel-jacket retrofitted reinforced concrete columns with recycled aggregate concrete", *Constr. Build. Mater.*, **158**, 624-639.

Holschemacher, K. (2004), "Hardened material properties of self-compacting concrete", *J. Civil Eng. Manag.*, **10**, 261-266.

Khan, Q.S., Sheikh, M.N. and Hadi, M.N.S. (2016), "Axial compressive behaviour of circular CFFT: Experimental database and design-oriented model", *Steel Compos. Struct., Int. J.*, **21**(4), 921-947.

Lee, H.S. and Cho, Y.S. (2009), "Evaluation of the mechanical properties of steel reinforcement embedded in concrete specimen as a function of the degree of reinforcement corrosion", *Int. J. Fracture*, **157**, 81-88.

Li, C.Q. and Melchers, R.E. (2005), "Time-dependent risk assessment of structural deterioration caused by reinforcement corrosion", *ACI Struct J.*, **102**, 754-762.

Li, D.W., Wei, R., Xing, F., Sui, L.L., Zhou, Y.W. and Wang, W.Y. (2018), "Influence of Non-uniform corrosion of steel bars on the seismic behavior of reinforced concrete columns", *Constr. Build. Mater.*, **167**, 20-32.

Liang, Q.Q. (2011), "High strength circular concrete-filled steel tubular slender beam–columns, Part I: Numerical analysis", *J. Constr. Steel Res.*, **67**, 164-171.

Liang, H.J., Li, S., Lu, Y.Y. and Yang, T. (2018), "The combined effects of wet–dry cycles and sustained load on the bond behavior of FRP–concrete interface", *Polym. Compos.* DOI: doi.org/10.1002/pc.24785

Liang, H.J., Li, S., Lu, Y.Y. and Hu, J.Y. (2019), "Electrochemical performance of corroded reinforced concrete columns strengthened with fiber reinforced polymer", *Compos. Struct.*, **207**, 576-588.

Lin, P.Z., Zhu, Z.C. and Li, Z.J. (1997), "Fire-resistant structure: the concrete filled steel tubular column", *Proceedings of the International Conference on Composite Construction-Conventional and Innovative*, pp. 397-401.

Liu, D.L. **(**2006), "Behaviour of eccentrically loaded high-strength rectangular concrete-filled steel tubular columns", *J. Constr. Steel Res.*, **62**, 839-846.

Lu, Y.Y., Liang, H.J., Li, S. and Li, N. (2015a), "Axial behavior of RC columns strengthened with SCC filled square steel tubes", *Steel Compos. Struct., Int. J.*, **18**(3), 623-639.

Lu, Y.Y., Liang, H.J., Li, S. and Li, N. (2015b), "Eccentric strength and design of RC columns strengthened with SCC filled steel tubes", *Steel Compos. Struct., Int. J.*, **18**(4), 833-852.

Lu, Y.Y., Hu, J.Y., Li, S. and Tang, W.S. (2018), "Active and passive protection of steel reinforcement in concrete column using carbon fibre reinforced polymer against corrosion", *Electrochimica Acta*, **278**, 124-136.

Maaddawy, T.A.E. and Soudki, K.A. (2003), "Effectiveness of Impressed Current Technique to Simulate Corrosion of Steel Reinforcement in Concrete", *J. Mater. Civil Eng.*, **15**(1), 41-47.

Priestley, M.J.N., Seible, F., Xiao, Y. and Verma, R. (1994a), "Steel jacket retrofitting of reinforced concrete bridge columns for enhanced shear strength-part 1: Theoretical considerations and test design", *ACI, Struct. J.*, **91**, 394-405.

Priestley, M.J.N., Seible, F., Xiao, Y. and Verma, R. (1994b), "Steel jacket retrofitting of reinforced concrete bridge columns for enhanced shear strength-part 2: Test results and comparison with Theory", *ACI, Struct. J.*, **91**, 537-551.

Qiao, D., Nakamura, H., Yamamoto, Y. and Miura, T. (2015), "Evaluation Method of Tensile Behavior of Corroded Reinforcing Bars Considering Radius Loss", *J. Adv. Concr. Technol.*, **13**, 135-146.

Rupp, J., Sezen, H. and Chaturvedi, S. (2014), "Axial behavior of steel-jacketed concrete columns", *Steel Compos. Struct., Int. J.*, **16**(1), 61-77.

Sezen, H. and Miller, E.A. (2011), "Experimental evaluation of axial behavior of strengthened circular reinforced-concrete columns", *J. Bridge Eng. ASCE*, **16**, 238-247.

Smith, J.L. and Virmani, Y.P. (2000), Materials and methods for corrosion control of reinforced and prestressed concrete structures in new construction", Report No. FHWA-RD-0081.

Tao, Z. and Han, LH. (2007), 'Behaviour of fire-exposed concrete-filled steel tubular beam columns repaired with CFRP wraps", *Thin-Wall. Struct.*, **45**(1), 63-76

Teng, J.G. and Lam, L. (2004), "Behavior and Modeling of Fiber Reinforced Polymer-Confined Concrete", *J. Struct. Eng.*, **130**(11), 1713-1723.

Wang, J., Liu, W.Q. and Zhou, D. (2014), "Mechanical behaviour of concrete filled double skin steel tubular stub columns confined by FRP under axial compression", *Steel Compos. Struct., Int. J.*, **17**, 431-452.

Xiao, Y. and Wu, H. (2003), "Strengthening of reinforced concrete columns using partially stiffened steel jackets", *J. Struct. Eng. ASCE*, **129**, 725-732.

Yadav, M., Sharma, D. and Kumar, S. (2015), "Thiazole derivatives as efficient corrosion inhibitor for oil-well tubular steel in hydrochloric acid solution", *Korean J. Chem. Eng.*, **32**, 993-1000.

Zhang, W.P., Song, X.B., Gu, X.L. and Li, S.B. (2012), "Tensile and fatigue behavior of corroded rebar", *Constr. Build. Mater.*, **34**(5), 409-417.

Zhang, F., Lu, Y.Y., Li, S. and Zhang, W.L. (2018), "Eccentrically compressive behaviour of RC square short columns reinforced with a new composite method", *Steel Compos. Struct., Int. J.*, **27**(1), 95-108.

Zhong, S.T. (2003), *The Concrete-Filled Steel Tubular Structures*, (3rd Ed.), Tsinghua University Press, Beijing, China. [In Chinese]

*CC*